Tellus (1991), *43A*, 213–225

Intraseasonal variations of the tropical easterly jet during the 1979 northern summer

By TSING-CHANG CHEN and MING-CHENG YEN, *Atmospheric Science Program, Department of Geological and Atmospheric Sciences, Iowa State University, Ames, Iowa 50011, USA*

(Manuscript received 23 August 1990; in final form 19 November 1990)

ABSTRACT

Numerous studies have investigated the intraseasonal oscillation of various elements of the Indian monsoon, but the tropical easterly jet has been neglected. The 1979 summer data generated by the FGG III-b analysis of the European Center for Medium Range Weather Forecasts were used to examine the intraseasonal oscillation of this jet. It was found that the jet possesses a distinctive intraseasonal oscillation south of its core. Previous studies suggested that the temporal fluctuation of this jet may be related through cumulus convection to that of the low-level Indian monsoon circulation. It was demonstrated by a streamfunction budget analysis that the intraseasonal oscillation of the tropical easterly jet south of its core is primarily induced by the eastward-propagating intraseasonal oscillation of the planetary-scale divergent circulation.

1. Introduction

As delineated by Krishnamurti and Bahlme (1976) (Fig. 1), the two most conspicuous components of the Indian monsoon circulation are the low-level Somali jet and the upper-level tropical easterly jet. More than three decades ago, Koteswaram (1958) pointed out that the time fluctuation of the tropical easterly jet is related to that of the low-level Indian monsoon. It may be inferred from Fig. 1 that temporal variations of these two jets are correlated through cumulus convection over central India. Plausibly, a mechanism inducing the time variation of convective activity over this region is reflected not only in that of the Somali jet, but also in that of the tropical easterly jet. Krishnamurti and Bahlme have extensively analyzed the short time-scale (<6 days), quasi-biweekly oscillations of the two jets, and other components of the Indian monsoon system (Fig. 1). Later, using the zonal winds generated by the FGGE III-b analyses of the European Center for Medium Range Weather Forecasts, Murakami et al. (1984a) examined the propagation and vertical structure of zonal wind associated with the 40–50 day oscillation over the Asian monsoon region. Although a surge of studies examining various aspects of the tropical intraseasonal oscillation has occurred in the past decade, few efforts have been made to explore the possible intraseasonal oscillation of the tropical easterly jet.

After the Monsoon Experiment (MONEX) data became available, Krishnamurti and Subrahmanyam (1982) depicted synoptically the northward migration of the 30–50 day transient Indian monsoon troughs and ridges originating around the equator. They found that the intensification (weakening) of the Somali jet synchronizes with the arrival of the 30–50 day transient monsoon troughs (ridges) at 20° N. Using the upper-level 30–50 day velocity potential (χ) anomalies, Krishnamurti et al. (1985), and Chen et al. (1988a) showed that this planetary-scale χ low-frequency mode propagates northeastward over the Indian monsoon area induces the transient Hadley circulation. Through this circulation, the planetary-scale 30–50 day mode couples with the low-level 30–50 day transient monsoon troughs and ridges and steers these troughs and ridges northward. These northward-traveling 30–50 day troughs and ridges interact with the stationary Indian monsoon trough located in central India and cause the latter's deepening and filling. Earlier, Chen and Yen (1986) found that the intensification (weakening) of the Somali jet is attributable to the deepening (filling) of the

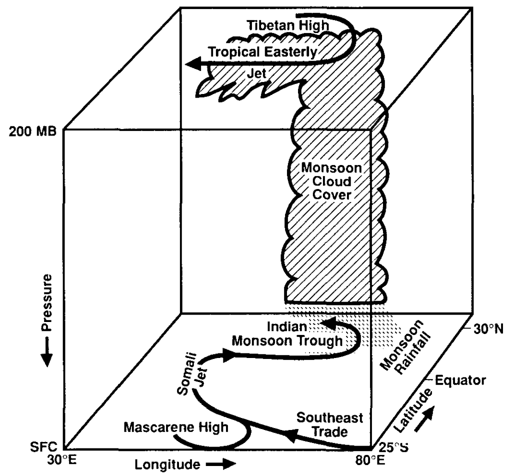

Fig. 1. A schematic diagram illustrating significant components of the Indian monsoon system (from Krishnamurti and Blahme, 1976).

stationary Indian monsoon trough over central India when the northward-traveling 30–60 day troughs (ridges) reach 20° N. The time evolution of the stationary Indian monsoon trough results in the intensification and weakening of the Indian monsoon and establishes its life cycle.

Murakami et al. (1984b), Cadet and Greco (1987), and Chen et al. (1988b) showed that the 30–50 day oscillation of the Somali jet modulates the water vapor transport, to the Indian subcontinent. Thus, this 30–50 day oscillation of water vapor transport, together with the cloud band associated with the northward-migrating 30–50 day troughs, causes the 30–50 day fluctuation of the Indian monsoon rainfall, as observed by Hartmann and Michelsen (1989). According to Koteswaram (1958), and implicit in Fig. 1, the tropical easterly jet may respond with a 30–50 day oscillation to convective activity over central India. This speculation leads us to question how the temporal variation of the tropical easterly jet behaves and how the temporal variations of the Somali jet and the tropical easterly jet are correlated through cumulus convection.

As discussed previously, the effect of the eastward-propagating planetary-scale 30–50 day mode on the low-level Indian monsoon has become clear in the past decade, although the interaction between them is a complicated process. Nevertheless, we question whether, in addition to what Koteswaram suggested, there may be an interaction between the planetary-scale 30–50 day mode and the tropical easterly jet that causes the latter's 30–50 day oscillation.

After analyzing for 1967 summer the kinetic energy budget of the tropical easterly jet in terms of the 200-mb wind fields, Chen (1982) suggested that the kinetic energy of this jet is generated on the upstream side, and then transported to the downstream side of the jet and destroyed. Chen and Van Loon (1987) later showed that the divergent (convergent) center of the east-west Walker circulation exists on the upstream (downstream) side of the tropical easterly jet and coincides with the divergent (convergent) center of the kinetic energy flux associated with this jet. It is likely that the northeastward propagation of the 30–50 day planetary-scale divergent circulation over the monsoon region may perturb the east-west Walker circulation associated with the tropical easterly jet, thus resulting in its intraseasonal oscillation.

The tropical easterly jet may be well delineated by streamfunction, which can be obtained by performing the inverse of the Laplacian on vorticity. Based upon the vorticity equation, the temporal variation of steamfunction can be induced through vorticity source, i.e., the divergence of vorticity flux by divergent flow. We shall therefore apply the streamfunction budget analysis (Kang and Held, 1987; Chen and Chen, 1990) to explore a possible interaction between the tropical easterly jet and the planetary-scale 30–50 day mode, which are well portrayed by anomalies. In this study, we shall use the 1979 summer data generated by the FGGE III-b analysis of the European Centre for Medium Range Weather Forecasts (ECMWF).

2. Intraseasonal oscillation* of the tropical easterly jet

The latent heat released by cumulus convection contributes to most tropical diabatic heating. This

* In order to be consistent with the historical account, the "30–50 day" oscillation was used in the Introduction. The "30–60 day" Butterworth bandpass filter was actually employed in computations of this study. The "30–60 day" oscillation is therefore adapted hereafter in this paper.

contribution can be inferred from analyses of outgoing longwave radiation (OLR) observed by satellite (e.g., Liebmann and Hartmann, 1981) and from the water-vapor budget analysis (e.g., Chen, 1985). According to the χ-maintenance equation developed by Chen (1989), the northern summer-mean divergent circulation, $(\bar{\chi}, \nabla\bar{\chi})$ (200 mb) (Fig. 2a), is primarily maintained by the diabatic heating centered at the South China Sea, where the upward branch of the east-west Walker circulation exists. Over the Asian monsoon region, the upper-level circulation depicted by streamlines consists of the South Asian high to the north of the equator and of the Indian Ocean high to the south of the equator. The tropical easterly jet straddles the contiguous region between these two high systems. The diabatic heating source associated with the summer monsoon is asymmetric with respect to the equator. Using the equatorial wave theory, Young (1987) illustrated that the response of tropical circulation to the monsoon diabatic heating is confined to the heat source region and the adjacent western areas with Rossby and mixed Rossby-gravity wave character. The contrast between $(\bar{\chi}, \nabla\bar{\chi})$ (200 mb) and $\bar{\mathbb{V}}$ (200 mb) over the Asian monsoon region suggests that Young's illustration may also explain the formation of this monsoon system.

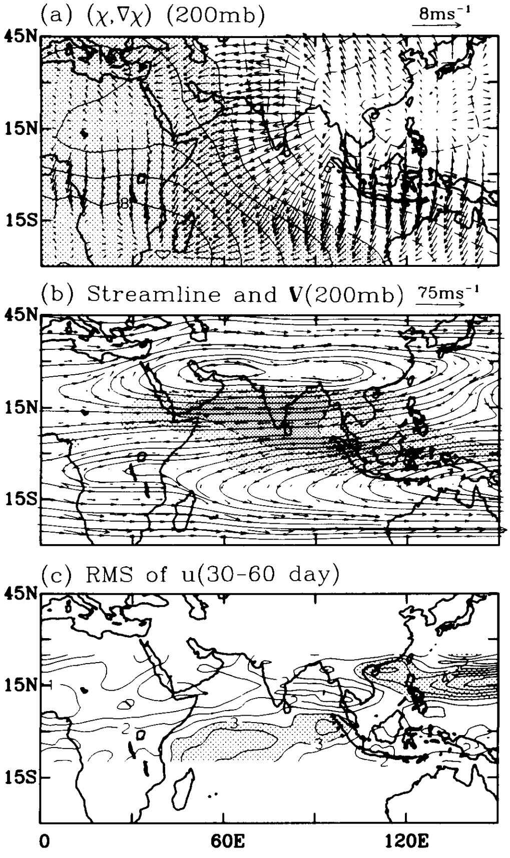

Fig. 2. Climatology of the upper-level monsoon circulation during 1979 northern summer: (a) divergent circulation $(\bar{\chi}, \nabla\bar{\chi})$ (200 mb), where $\bar{\chi}$ is velocity potential and $\nabla\bar{\chi}$ is divergent wind vector ($\bar{V}_D$); (b) streamlines at 200 mb and wind vector [$\bar{V}$(200 mb)]; and (c) the root mean square (RMS) of the 30–60 day filtered $\bar{u}$ (200 mb). In (a), the positive values of $\bar{\chi}$ are shaded and the $\bar{\chi}$ (200 mb) contour interval is $2 \times 10^7\,m^2\,s^{-1}$. In (b), $|\bar{V}(200\,mb)| \geq 15\,ms^{-1}$ is heavily shaded and $15\,ms^{-1} \geq |\bar{V}(200\,mb)| \geq 10\,ms^{-1}$ is lightly shaded. The contour interval of u (200 mb) RMS is $1\,ms^{-1}$, and $\bar{u}$ (200 mb) RMS $\geq 3\,ms^{-1}$ is shaded.

It was demonstrated by Chen et al. (1988a) that the monsoon life cycle is generated by the modulation of the eastward-propagating 30–60 day mode on the monsoon developed by the annual heating cycle. Based upon either the energetic interaction between rotational and divergent flows that was proposed by Chen and Wiin-Nielsen (1976) or the tropical monsoon circulation formed by equatorial waves that was suggested by Young (1987), we may infer from the synoptic relation between the upper-level monsoon divergent and rotational circulations depicted previously that the eastward-propagating 30–60 day χ oscillation may perturb and cause the low-frequency oscillation of the upper-level monsoon circulation. In particular, the tropical easterly jet may undergo this low-frequency oscillation induced in some way by the 30–60 day χ oscillation. The root mean square (RMS) of the 30–60 day filtered u(200 mb) field (Fig. 2c) suggests that the most significant 30–60 day oscillation of the tropical easterly jet appears in the southern part of jet. Magaña and Yanai (1990) delineated the time evolution of the South Asian high affected by the 30–60 day oscillation. In contrast, Chen (1985) analyzed the T(200 mb) temperature field over the Tibetan high but did not find a pronounced 30–60 day oscillation of this thermal field during the monsoon season. The small variance of 30–60 day filtered u(200 mb) over this region is consistent with Chen's findings.

Koteswaram (1958) argued that the fluctuation of the tropical easterly jet is related to the fluctuation of the low-level Indian monsoon circulation. Sikka and Gadgil (1980), Krishnamurti et al. (1985), Chen et al. (1988a), and others have found that cumulus convection associated with the Indian monsoon trough over central India exhibits a 30–60 day oscillation. As can be inferred from Krishnamurti and Blahme's (1976) schematic diagram of the Indian monsoon system, the northern part of the tropical easterly jet may possess this low-frequency oscillation through the suggested link to cumulus convection. But, Fig. 2c demonstrates that this is not the case. Seemingly, the mechanism inducing the possible 30–60 day oscillation in the southern part of the tropical easterly jet differs from the linkage speculated upon here.

To develop a clearer view of the 30–60 day oscillation of the tropical easterly jet, time series of u(200 mb) (solid lines), along 75° E for every 5° latitude, ranging from 10° S to 20° N, are displayed in Fig. 3. The dotted curves are a combination of the summer (May–September)-mean and seasonal cycle components of u(200 mb) obtained by a least-square fit, whereas the oscillatory dashed curves represent a sum of the summer mean, seasonal cycle, and the 30–60 day filtered u(200 mb). Let us denote the former combination by (ˆ) and the 30–60 day component by (˜). A pronounced $\tilde{u}$(200 mb) signal appears from 5° N southward until easterlies become insignificant around 10° S, where the ridge line of the Indian Ocean high (Fig. 2b) is located. The maximum amplitude of $\tilde{u}$(200 mb) can reach 6 ms^{-1} at 5° S.

The intensity of the Somali jet is highly correlated both with the arrival of transient monsoon troughs and ridges at 20° N from the equator (Krishnamurti and Subrahmanyam, 1982) and with the deepening and filling of the Indian monsoon trough (Chen and Yen, 1985). Accordingly, we use the area-mean height Z(850 mb) over central India, which covers a part of the Indian monsoon trough, as an index of the 30–60 day oscillation of the low-level Indian monsoon, particularly of the Somali jet, to better outline the relation between the Somali and tropical easterly jets. The contrast between the time series of monsoon area-mean [$\hat{Z}$(850 mb) + $\tilde{Z}$(850 mb)] and [$\hat{u}$(200 mb) + $\tilde{u}$(200 mb)] around the equator (5° N, 0°, 5° S) seemingly indicates that the intensity variations of these two jets are in phase to a great extent. To objectify this assessment, we com-

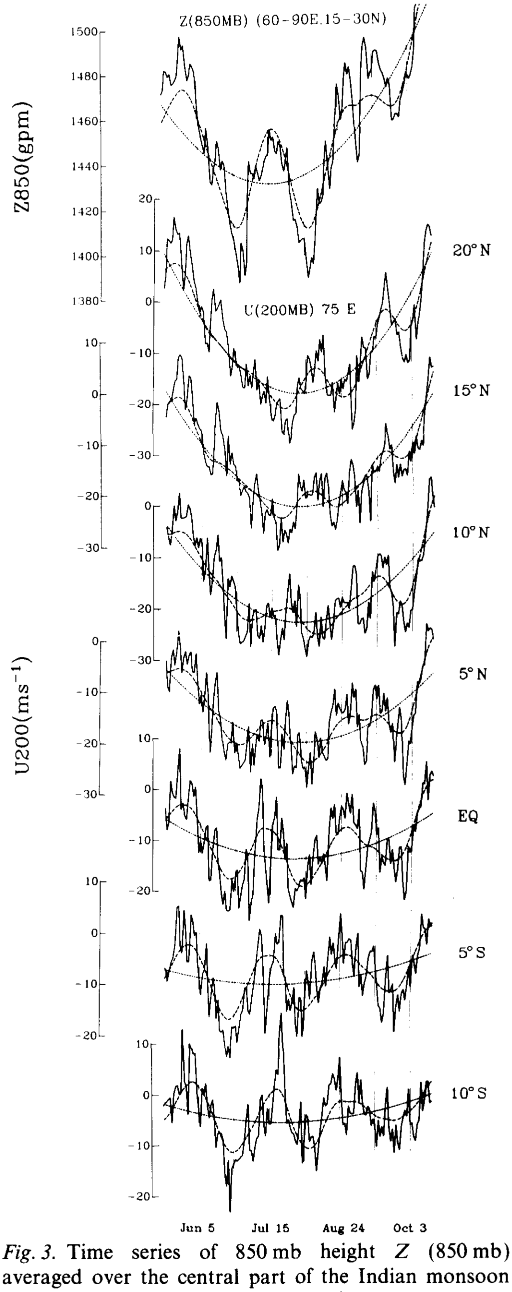

Fig. 3. Time series of 850 mb height Z (850 mb) averaged over the central part of the Indian monsoon trough within the region of (60°–90° E, 15°–30° N) and of u (200 mb) along 75° E every 5° latitude, ranging from 20° N to 10° S. The solid curves are the real-time series of area-mean Z (850 mb) and u (200 mb). The dotted curves represent a combination of summer (10 May–15 October)-mean, (¯), and seasonal cycle, (ˆ), determined by a least square fitting. The dashed curves are sum of (¯), (ˆ), and the 30–60 day component, (˜).

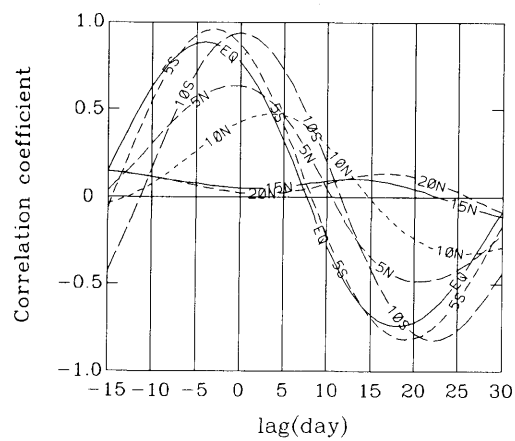

Fig. 4. Correlation coefficients between area-mean $\tilde{Z}$ (850 mb) and $\tilde{u}$ (200 mb) along 75°E at various latitudes with different lags.

pute with different lags the lag-correlation coefficients between these two time series. As shown in Fig. 4, the maximum correlation coefficient between the two time series occurs with lag of about ±3 days. Surely, the 30–60 day oscillation of the Somali and tropical easterly jets are more or less in phase.

3. A possible explanation of the low-frequency oscillation associated with the tropical jet stream

The northern part of the tropical easterly jet, as revealed from Figs. 2c and 3, does not exhibit a significant 30–60 day oscillation. Thus, it can be inferred that the pronounced impact of the 30–60 day mode on the low-level Indian monsoon system does not exert any significant regional effect on the tropical easterly jet through a direct interaction between these two elements of monsoon circulation. On the other hand, as shown in Fig. 4, the 30–60 day oscillation of the low-level Indian monsoon circulation and the 30–60 day oscillation associated with the southern part of the tropical easterly jet almost synchronize. Previous studies, e.g., Krishnamurti et al. (1985) and Chen et al. (1988a), have shown that the 30–60 day oscillation of the low-level monsoon circulation is essentially induced by the eastward-propagating 30–60 day mode. The synchronization between the intraseasonal oscillations of the two jets may suggest that the 30–60 day oscillation of the tropical easterly jet is attributed to a direct interaction between the eastward-propagating 30–60 day χ mode and the upper-level monsoon circulation, which includes the tropical easterly jet. To prove this hypothetical possibility, we shall perform the streamfunction budget analysis (Kang and Held, 1987; Chen and Chen, 1990) of the upper-level monsoon circulation.

3.1. Synoptics

Before engaging the streamfunction budget analysis in detail, we ought to understand the synoptic structure of the 30–60 day rotational and divergent circulations for various phases of the monsoon system. We use [$\hat{u}$(200 mb) + $\tilde{u}$(200 mb)] at (25°E, 0°) as an index by which to select three minimum phases (30 May–3 June, 11–15 July, 22–26 August) and two maximum phases (20–24 June, 31 July–4 August) of the tropical easterly jet. Accordingly, we display five-day averaged $\tilde{\mathbf{V}}_R$ (200 mb) (Fig. 5c), $\tilde{\psi}$ (200 mb) (Fig. 5b), and [$\tilde{\chi}, \nabla\tilde{\chi}$) (200 mb), O$\tilde{\text{L}}$R (Fig. 5a) for the selected five phases. Regardless of the complicated $\tilde{\mathbf{V}}_R$ (200 mb) structurer over East Asia, a simple alternation of the 30–60 day northeasterly and southwesterly anomalies exists between north of 15°S and south of 5°N. This alternation of $\tilde{\mathbf{V}}_R$ (200 mb) direction, which of course includes the $\tilde{\mathbf{V}}_R$ (200 mb) magnitude as well, constitutes the 30–60 day oscillation of the southern part of the tropical easterly jet. The $\tilde{\mathbf{V}}_R$ (200 mb) anomalies can be well represented by $\tilde{\psi}$ (200 mb) (Fig. 5b), which exhibits a clear north-south alternation between positive and negative $\tilde{\psi}$ (200 mb) anomalies. Note that the positive (negative) $\tilde{\psi}$ (200 mb) anomalies denote clockwise (counterclockwise) rotational flow. The main concern of the current study is to examine whether alternation of the $\tilde{\psi}$ (200 mb) anomalies associated with the easterly jet during various phases of the jet's time evaluation can be induced by the eastward-propagating 30–60 day χ mode.

Displayed in Fig. 5a are the five-day averaged ($\tilde{\chi}, \nabla\tilde{\chi}$) (200 mb) and O$\tilde{\text{L}}$R anomalies for five selected phases of the 30–60 day oscillation of the tropical easterly jet. When the southwesterly (northeasterly) anomalies of $\tilde{\mathbf{V}}_R$ (200 mb) that are associated with the southern part of the tropical easterly jet reach their maximum, a divergent (con-

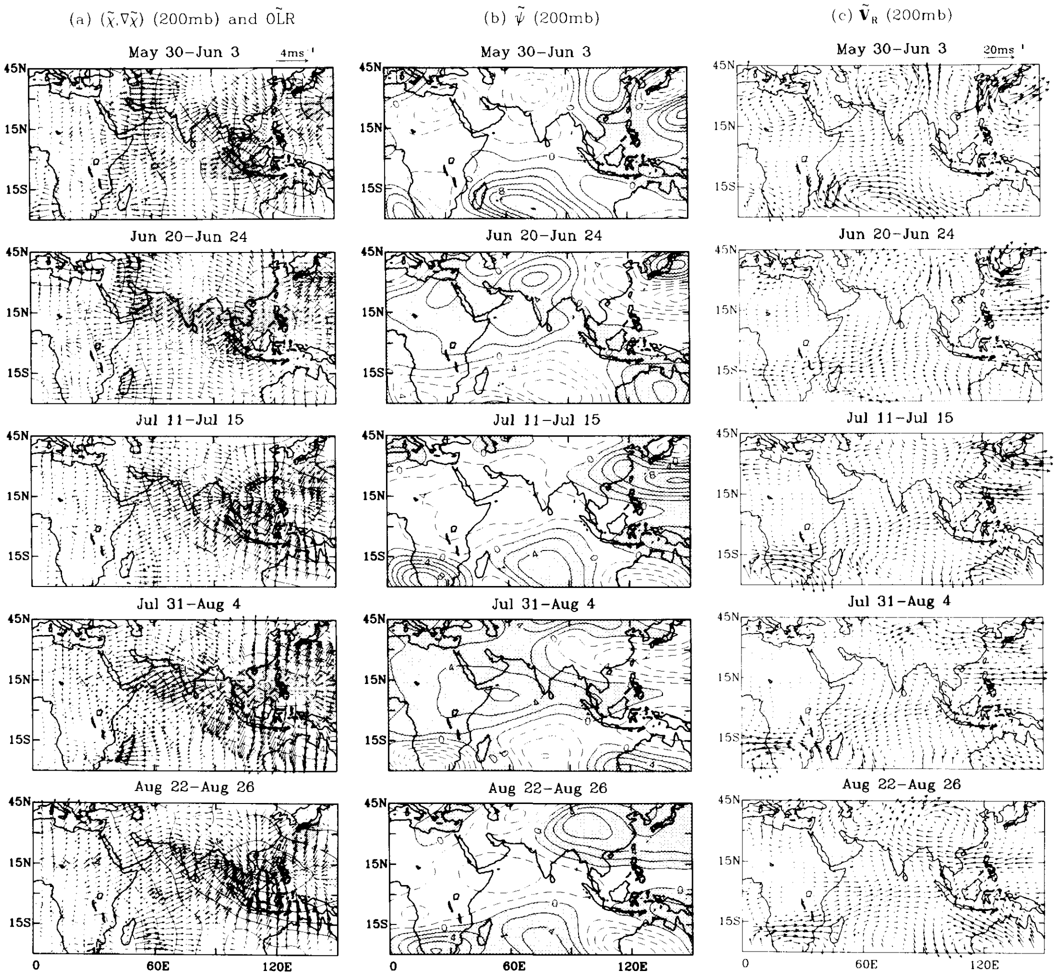

Fig. 5. The 5-day averaged synoptic charts of (a) $(\tilde{\chi}, \nabla\tilde{\chi})$ (200 mb) superimposed with $\widetilde{OLR}$, (b) 30–60 day filtered streamfunction $\tilde{\psi}$ (200 mb), and (c) 30–60 day filtered rotational wind vector $\tilde{V}_R$ (200 mb) for various phases of the 30–60 day oscillation of the tropical easterly jet. The contour intervals of $\tilde{\chi}$ (200 mb) and $\tilde{\psi}$ (200 mb) are 10^6 m^2 s^{-1}, respectively. $\widetilde{OLR} \leqslant -10$ ($\geqslant 10$) Watt m^{-2} is heavily (lightly) shaded. Positive $\tilde{\psi}$ (200 mb) anomalies are shaded in (b).

vergent) center of $(\tilde{\chi}, \nabla\tilde{\chi})$ (200 mb) is located over the South China Sea and a minor convergent (divergent) center of $(\tilde{\chi}, \nabla\tilde{\chi})$ (200 mb) over South Africa. Moreover, the negative (heavy-shaded) and positive (light-shaded) $\widetilde{OLR}$ anomaly bands alternate in the north-south direction. The negative (positive) $\widetilde{OLR}$ anomaly band extends from the Arabian Sea eastward, across the Indian subcontinent and Indochina, to the South China Sea and the western Pacific; and when the southern part of the tropical easterly jet reaches its maximum (minimum), a minor positive (negative) $\widetilde{OLR}$ anomaly band locates around the equator south of India. According to Sikka and Gadgil (1980), Krishnamurti et al. (1985), Chen et al. (1988a), the Somali jet intensifies as the cloud band associated with the transient monsoon troughs migrates northward to central India. Therefore, the synoptic relations among $(\tilde{\chi}, \nabla\tilde{\chi})$ (200 mb), $\widetilde{OLR}$, and $\tilde{\psi}$ (200 mb) revealed from

Fig. 5 make clear once again the synchronization of the 30–60 day oscillations of the tropical easterly and Somali jets.

The last issue we will address is how the eastward-propagating 30–60 day χ mode interacts with the upper-level monsoon circulation to induce the 30–60 day oscillation of the latter. In the past, Krishnamurti and Ramanathan (1982) and Chen and Yen (1986) applied the energetics scheme of rotational and divergent flows proposed by Chen and Wiin-Nielsen (1976) to examine the effect of the 30–60 day χ mode on the low-level monsoon circulation. The energetics analysis, of course, sheds light on the physical processes stimulating this 30–60 day oscillation. Nevertheless, the energetics analysis cannot provide information concerning the change of flow direction. Because the streamfunction, whose gradients are horizontal winds, is often used to portray atmospheric flow, the streamfunction budget analysis is a more proper method of illustrating the interaction between intraseasonal χ and ψ modes.

3.2. *Streamfunction budget analysis*

3.2.1. Formulation. The vorticity equation may be written as

$$\frac{\partial \zeta}{\partial t} = -\boldsymbol{V}_\psi \cdot \nabla(\zeta + f) - \nabla \cdot [\boldsymbol{V}_\chi(\zeta + f)] + F. \tag{1}$$

The notation used here is conventional. Vorticity advection by divergent flow is combined with vortex stretching to form vorticity source, the second term on the right-hand side of (1). F includes vertical advection, twisting, and dissipation of vorticity. To examine the 30–60 day streamfunction budget, we first compute the daily budget of vorticity departure from its seasonal mean, ζ', where $(\ )' = (\ ) - (\bar{\ })$ and $(\bar{\ })$ = seasonal mean, with the equation

$$\frac{\partial \zeta'}{\partial t} = -\bar{\boldsymbol{V}}_\psi \cdot \nabla\zeta' - \boldsymbol{V}_{\psi'} \cdot \nabla(\bar{\zeta} + f) \underset{\text{(a)}}{- \boldsymbol{V}_{\psi'} \cdot \nabla\zeta'} \underset{\text{(b)}}{- \overline{\boldsymbol{V}_{\psi'} \cdot \nabla\zeta'}} - \nabla \cdot [\boldsymbol{V}_{\chi'}(\bar{\zeta} + f)] + \nabla \cdot (\bar{\boldsymbol{V}}\zeta') \underset{\text{(c)}}{+ \nabla \cdot (\boldsymbol{V}_{\chi'}\zeta')} \underset{\text{(d)}}{- \nabla \cdot \overline{(\boldsymbol{V}_{\chi'}\zeta')}}] + F'. \tag{2}$$

Eq. (2) is essentially a linear equation in time, except that, as revealed from our diagnostic computation terms, (a) and (c) are much smaller than the other terms. The transient streamfunction budget can be obtained by performing the inverse of the Laplacian on (2):

$$\frac{\partial \psi'}{\partial t} = \underbrace{-\nabla^{-2}[\bar{\boldsymbol{V}}_\psi \cdot \nabla\zeta' + \boldsymbol{V}_{\psi'} \cdot \nabla(\bar{\zeta} + f) - \boldsymbol{V}_{\psi'} \cdot \nabla\zeta' - \overline{\boldsymbol{V}_{\psi'} \cdot \nabla\zeta'}]}_{\psi'_{\mathrm{AV}}} \underbrace{-\nabla^{-2}\{\nabla \cdot [\boldsymbol{V}_{\chi'}(\bar{\zeta} + f)] + \nabla \cdot (\bar{\boldsymbol{V}}\zeta') + \nabla \cdot (\boldsymbol{V}_{\chi'}\zeta') - \nabla \cdot \overline{(\boldsymbol{V}'\zeta')}]}_{\psi'_\chi} \underbrace{+\nabla^{-2}F'}_{\psi'_F}. \tag{3}$$

We then apply the 30–60 day Butterworth bandpass filter to (3) to obtain the $\tilde{\psi}$ budget

$$\frac{\partial \tilde{\psi}}{\partial t} = \underbrace{-\nabla^{-2}[\bar{\boldsymbol{V}}_\psi \cdot \nabla\tilde{\zeta} + \tilde{\boldsymbol{V}}_\psi \cdot \nabla(\bar{\zeta} + f) - \boldsymbol{V}_{\psi'} \nabla\zeta']}_{\tilde{\psi}_{\mathrm{AV}}} \underbrace{-\nabla^{-2}\{\nabla \cdot [\tilde{\boldsymbol{V}}_\chi(\bar{\zeta} + f)] + \nabla \cdot (\bar{\boldsymbol{V}}\tilde{\zeta}) + \nabla \cdot (\boldsymbol{V}_{\chi'}\zeta')\}}_{\tilde{\psi}_\chi} \underbrace{+\nabla^{-2}\tilde{F}}_{\tilde{\psi}_F}. \tag{4}$$

Note that the nonlinear interaction terms, $-\nabla^{-2}(\boldsymbol{V}_{\psi'} \cdot \nabla\zeta')$ and $-\nabla^{-2}[\nabla \cdot (\boldsymbol{V}_{\chi}, \zeta)]$, include contributions from interactions between various time-scale modes to the 30–60 day mode. The reason of computing these terms with this approach is because we would like to take the nonlinear-interaction effect into account with a manageable computation. Therefore, (2)–(4) were used in our $\tilde{\psi}$ budget analysis. $\tilde{\psi}_{\mathrm{AV}}$ is the $\tilde{\psi}$ tendency induced by vorticity advection by rotational flow, whereas $\tilde{\psi}_\chi$ is the $\tilde{\psi}$ tendency induced by vorticity source associated with the 30–60 day mode. As revealed from our computations, $\tilde{\psi}_F$ is generally much smaller than $\tilde{\psi}_{\mathrm{AV}}$ and $\tilde{\psi}_\chi$. Moreover, the time evolution of $\tilde{\psi}_F$ (not shown) does not possess such a coherent relationship with that of $\tilde{\psi}$ as time-evolutions of $\tilde{\psi}_{\mathrm{AV}}$ and $\tilde{\psi}_\chi$. Thus, we shall focus on $\tilde{\psi}_{\mathrm{AV}}$ and $\tilde{\psi}_\chi$. Based upon scale analysis and upon our diagnostic computation, which will be presented later, the approximation

$$\tilde{\psi}_{\chi} \simeq -\nabla^{-2}[\nabla\cdot(\tilde{V}_{\chi}f)] = \tilde{\psi}_{\chi 1} \tag{5}$$

is legitimate. Because f is only a function of latitude, $\tilde{\psi}_{\chi 1}$ provides us a direct channel for exploring the effect of the 30–60 day χ mode on the time evolution of the $\tilde{\psi}$ field.

We focus our analysis on the 200 mb level. To obtain ψ'_{AV} and ψ'_{χ}, we perform the daily computation of all vorticity advection and vorticity source terms and solve the Poisson equations in terms of the spectral method, with a horizontal triangular truction of 31 waves (T31). With this approach, we do not encounter the difficulty of boundary conditions at the poles.

3.2.2. Results of the $\tilde{\psi}$-budget analysis. The *y–t* diagrams of $\tilde{\psi}$, $\tilde{\chi}$, $\tilde{\psi}_{AV}$, $\tilde{\psi}_{\chi}$, and $\tilde{\psi}_{\chi 1}$ at 200 mb averaged from 72.5° to 77.5° E, i.e., centered at 75° E, are displayed in Fig. 6. A clear north-south alternation with a period of about 45 days between positive and negative $\tilde{\psi}$ anomalies around the equator can be seen on the top panel. Because positive (negative) $\tilde{\psi}$ (200 mb) denotes anticyclonic (cyclonic) flow, the north-south alternation of $\tilde{\psi}$ at the equator reflects the alternation of east and west motions. If the 30–60 day $\tilde{\chi}$ mode propagates regularly eastward, the $\tilde{\chi}$ (200 mb) anomalies at 75° E must also exhibit an alternation of positive and negative $\tilde{\chi}$ (200 mb) anomalies with a period of about 45 days. The *y–t* diagram of $\tilde{\chi}$ (200 mb) shown in the second panel of Fig. 6 characterizes what is expected. The next question facing us is how the eastward-propagating $\tilde{\chi}$ mode induces the north-south alternation of $\tilde{\psi}$ over this monsoon region.

The third and fourth panels of Fig. 6 show that $\tilde{\psi}_{AV}$ (200 mb) and $\tilde{\psi}_{\chi}$ (200 mb) are opposite in sign. This means that, physically, the time evolution of the $\tilde{\psi}$ (200 mb) tendency induced by the vorticity source associated with the 30–60 day mode is followed by that of the $\tilde{\psi}$ (200 mb) tendency induced by horizontal vorticity advection by rotational flow. As mentioned earlier, $\tilde{\psi}_F$ (200 mb) is generally much smaller than either $\tilde{\psi}_{AV}$ (200 mb) or $\tilde{\psi}_{\chi}$ (200 mb). The $\tilde{\psi}$ (200 mb) tendency, i.e., the time evolution of $\tilde{\psi}$ (200 mb), should be primarily attributed to the mutual adjustment and counterbalance between $\tilde{\psi}_{\chi}$ (200 mb) and $\tilde{\psi}_{AV}$ (200 mb). According to (4), $\tilde{\psi}_{\chi}$

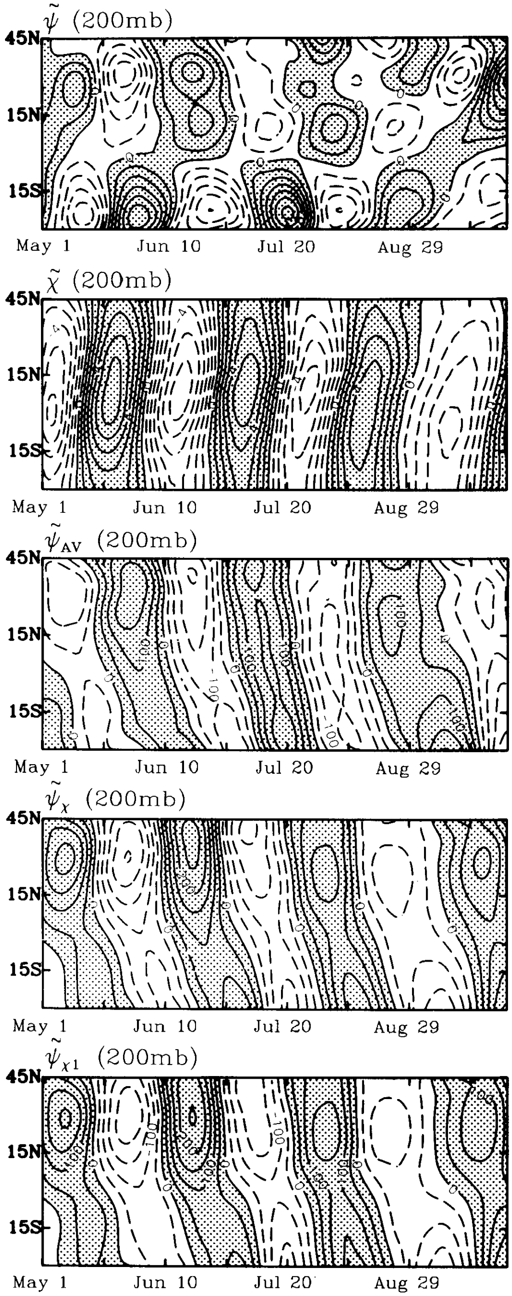

Fig. 6. The *y–t* diagrams of $\tilde{\psi}$ (200 mb), $\tilde{\chi}$ (200 mb), $\tilde{\psi}_{AV}$ (200 mb), $\tilde{\psi}_{\chi}$ (200 mb), and $\tilde{\psi}_{\chi 1}$ (200 mb) averaged between 72.5° E and 77.5° E, namely centered at 75° E. The contour intervals used are $\tilde{\psi}$ (200 mb) 2×10^6 $m^2\,s^{-1}$; $\tilde{\chi}$ (200 mb) 10^6 $m^2\,s^{-1}$ $\tilde{\psi}_{AV}$ (200 mb) 50 $m^2\,s^{-2}$; $\tilde{\psi}_{\chi}$ (200 mb) 50 $m^2\,s^{-2}$; and $\tilde{\psi}_{\chi 1}$ (200 mb) 50 $m^2\,s^{-2}$. The positive values of all quantities are shaded.

(200 mb) has a complicated mathematical expression. The contrast between the $\tilde{\psi}_\chi$ (200 mb) and $\tilde{\psi}_{\chi 1}$ (200 mb) *y–t* diagrams (Fig. 6), however, clearly shows that the $\tilde{\psi}$ (200 mb) tendency induced by vorticity source is more or less contributed by the vortex-stretching effect. Because *f* is only a function of latitude, the time evolution of $\tilde{\psi}_{\chi 1}$ (200 mb) must be caused completely by the $\tilde{V}_\chi$ (200 mb) or $\tilde{\chi}$ (200 mb) field. That is to say, the eastward-propagating $\tilde{\chi}$ mode induces the time evolution of either $\tilde{\psi}_{\chi 1}$ (200 mb) or $\tilde{\psi}_\chi$ (200 mb), which is in turn counterbalanced by the $\tilde{\psi}$ (200 mb) tendency induced by horizontal vorticity avection. The *y–t* diagrams of the $\tilde{\psi}$ (200 mb) budget at 75°E (Fig. 6) demonstrate that the north-south alternation of $\tilde{\psi}$ (200 mb) at the equator is attributable to the eastward-propagating $\tilde{\chi}$ (200 mb) mode.

Some interesting features regarding the *y–t* diagrams of the $\tilde{\psi}$ (200 mb) budget are worth mentioning. Careful examination of Fig. 6 reveals that $\tilde{\psi}_\chi$ (200 mb) is somewhat larger than $\tilde{\psi}_{AV}$, particularly north of the equator. Additionally, the time evaluations of $\tilde{\psi}$ (200 mb) and $\tilde{\psi}_\chi$ (200 mb) almost synchronize before the end of August. In contrast, the time evolutions of $\tilde{\psi}$ (200 mb) and $\tilde{\psi}_\chi$ (200 mb) or of $\tilde{\psi}$ (200 mb) and $\tilde{\psi}_{AV}$(200 mb) south of the equator are in quadrature; $\tilde{\psi}_\chi$(200 mb), $\tilde{\psi}$ (200 mb), and $\tilde{\psi}_{AV}$ (200 mb) lag behind $\tilde{\psi}$ (200 mb). Analyzing the streamfunction budget of stationary eddies ($\bar{\psi}_E$), Chen and Chen (1990) found that the $\bar{\psi}_E$ tendency induced by vorticity source ($\bar{\psi}_{\chi E}$) and by horizontal avection of vorticity ($\bar{\psi}_{AVE}$) are opposite in sign and spatially in quadrature with respect to the $\bar{\psi}_E$ structure. As shown in Fig. 6, the distinction between the $\tilde{\psi}$

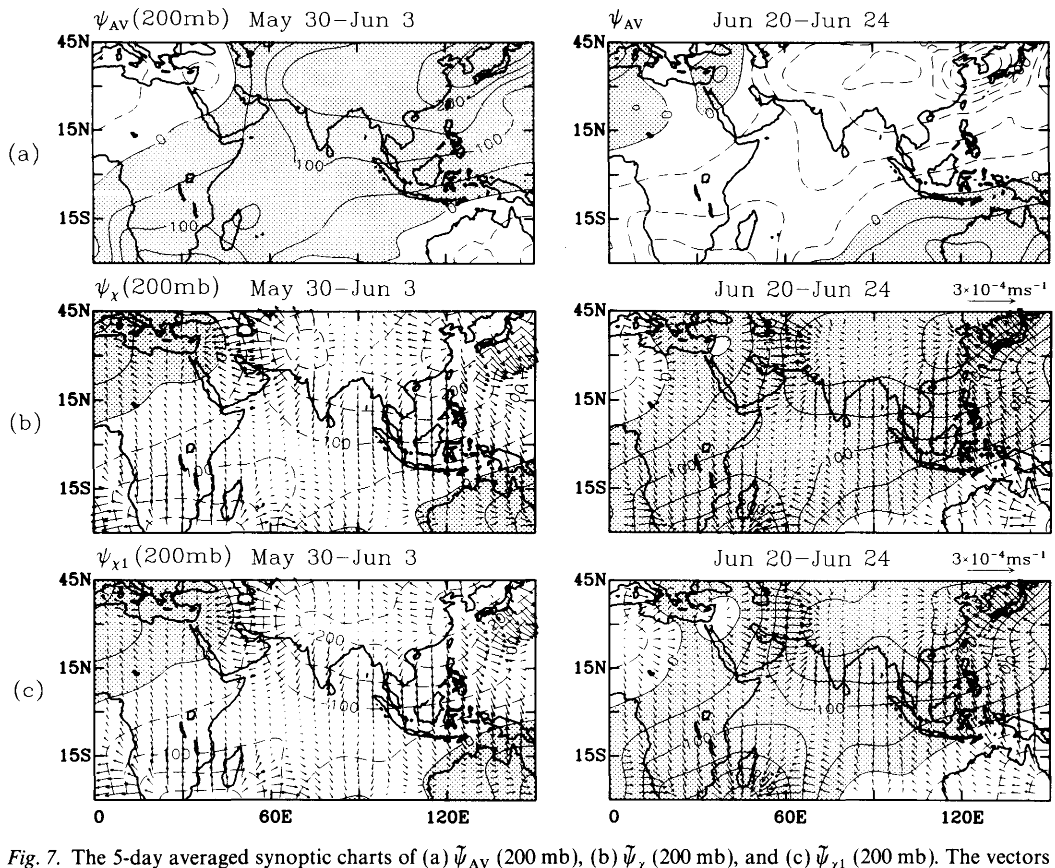

Fig. 7. The 5-day averaged synoptic charts of (a) $\tilde{\psi}_{AV}$ (200 mb), (b) $\tilde{\psi}_\chi$ (200 mb), and (c) $\tilde{\psi}_{\chi 1}$ (200 mb). The vectors displayed on (b) and (c) are $\nabla\tilde{\psi}_\chi$ and $\nabla\tilde{\psi}_{\chi 1}$, respectively, to indicate the $\tilde{\psi}$ tendency induced by the souce or sink of vorticity. The positive values of all quantities are shaded, and the contour interval of all quantities is 50 $m^2 s^{-2}$.

budgets north and south of the equator may be due to differences between monsoon and midlatitude dynamics; the $\tilde{\psi}$ (200 mb) budget north (south) of the equator is characterized by the monsoon (midlatitude) nature.

The y–t diagrams of the $\tilde{\psi}$ (200 mb) budget along 75° E provide only the local response of the $\tilde{\psi}$ (200 mb) field to the eastward-propagating $\tilde{\chi}$ mode. In order to gain an overview of this response over the entire monsoon region, the five-day averaged charts of $\tilde{\psi}_{AV}$ (200 mb), $\tilde{\psi}_{\chi}$ (200 mb), and $\tilde{\psi}_{\chi 1}$ (200 mb) during the first maximum (30 May–3 June) and minimum (20–24 June) phases of $\tilde{u}$ (200 mb) at (75° E, 0°)'s are shown in Fig. 7. The $\tilde{\chi}$ (200 mb) flip-flop oscillations (Fig. 3c) during the maximum and minimum phases of $\tilde{u}$ (200 mb) at (75° E, 0°) result in those of $\tilde{\psi}_{\chi 1}$ (200 mb) and $\tilde{\psi}_{\chi}$ (200 mb). The resemblence between $\tilde{\psi}_{\chi}$ (200 mb) and $\tilde{\psi}_{\chi 1}$ (200 mb) is not limited to 75° E, as revealed from Fig. 6, but exists over the entire domain of analysis. It was observed in Fig. 6 that time evolutions both of $\tilde{\psi}$ (200 mb) and $\tilde{\psi}_{\chi}$ (200 mb) and of $\tilde{\psi}$ (200 mb) and $-\tilde{\psi}_{AV}$ (200 mb) are in phase north of the equator along 75° E. This very feature of the $\tilde{\psi}$ (200 mb) budget also appears in Fig. 7. In contrast, south of the equator, the time evolution of $\tilde{\psi}_{\chi}$ (200 mb) or $\tilde{\psi}_{\chi 1}$ (200 mb) leads that of $\tilde{\psi}$ (200 mb); and $\tilde{\psi}_{AV}$ (200 mb) lags behind $\tilde{\psi}$ (200 mb). In other words, $\tilde{\psi}$ (200 mb) may reach its maximum and minimum when $\tilde{\psi}_{\chi}$ (200 mb) and $\tilde{\psi}_{AV}$ (200 mb) are in their transition periods. Moreover, it is also revealed from Fig. 7 that the spatial structures of $\tilde{\psi}_{AV}$ (200 mb) and $\tilde{\psi}_{\chi}$ (200 mb) south of the equator and midlatitudes over Northeast Asia and the Middle East behave similarly to the $\bar{\psi}_E$ budget analyzed by Chen and Chen (1990). Namely, we perceive that $\tilde{\psi}$ (200 mb) is spatially in quadrature with respect to $\tilde{\psi}_{\chi}$ (200 mb) and $\tilde{\psi}_{AV}$ (200 mb).

In summary, the most significant outcome of the $\tilde{\psi}$-budget analysis is that it demonstrates the possibility that the 30–60 day oscillation of the southern part of the tropical easterly jet is a response of the upper-level monsoon circulation to the eastward-propagating $\tilde{\chi}$ mode.

4. Concluding remarks

In the last decade, numerous studies have been devoted to examining the quasi-periodic fluctuations of various components of the Indian monsoon. It has been well documented that the 30–60 day oscillation exerts the most profound impact on the life cycle of the Indian monsoon system. The most distinctive element of the Indian monsoon is the tropical easterly jet. Although Krishnamurti and Bahlme (1976) examined the biweekly oscillation of this jet and Murakami et al. (1984) analyzed the low-frequency oscillation of zonal wind over the monsoon region, no attempt has been made to explore (1) whether the tropical easterly jet possesses a 30–60 day oscillation, (2) what mechanism may cause this intraseasonal oscillation, and (3) what the possible impact of this interseasonal oscillation would be on the monsoon or on the weather systems of adjacent regions.

The 1979 summer (May–September) data generated by the FGGE III-b analyses of the European Centre for Medium Range Weather Forecasts were used in this study to explore the three questions raised above. The southern part of the tropical easterly jet south of 5° N over the Indian Ocean was found to exhibit a 30–60 day oscillation with an amplitude of 6 ms^{-1} at (75° E, 5° S). This oscillation almost synchronizes with the 30–60 day oscillation of the Indian monsoon troughs; the latter couples with the 30–60 day oscillation of the low-level Indian monsoon circulation, particularly with that of the Somali jet. Krishnamurti et al. (1985) and Chen et al. (1988a) showed that the 30–60 day oscillation, i.e., the life cycle, of the low-level Indian monsoon circulation is primarily caused by the eastward propagating 30–60 day mode. Synchronization between the intraseasonal oscillations of the upper-level tropical easterly jet and the low-level Somali jet seems to suggest that the former oscillation is also induced by the eastward-propagating 30–60 day mode, instead of by direct coupling between these two jets. The large-scale upper-level monsoon atmospheric circulation, which includes the tropical easterly jet, can be well portrayed by streamfunction. A budget analysis of the 30–60 day streamfunction ($\tilde{\psi}$) anomalies at 200 mb over the monsoon region is performed to illustrate the effect of eastward-propagating divergent circulation mode on the time evolution of the monsoon $\tilde{\psi}$ field.

The y–t diagrams of various $\tilde{\psi}$ (200 mb)-budget quantities along 75° E were used to illustrate how the 30–60 day velocity potential ($\tilde{\chi}$) mode interacts with the upper-level monsoon flow to induce the 30–60 day oscillation of the tropical easterly jet. The $\tilde{\psi}$ (200 mb) tendency induced by the vorticity source [$\tilde{\psi}_\chi$ (200 mb)] is mostly contributed by that generated by the $\tilde{\chi}$ mode. This $\tilde{\psi}$ (200 mb) tendency, i.e., $\tilde{\psi}_\chi$ (200 mb), is counterbalanced by the $\tilde{\psi}$ (200 mb) tendency induced by horizontal vorticity advection with interseasonal oscillation [$\tilde{\psi}_{AV}$(200 mb)]. The mutual adjustment between $\tilde{\psi}_\chi$ (200 mb) and $\tilde{\psi}_{AV}$ (200 mb) results in the major part of the $\tilde{\psi}$ (200 mb) time evolution. Further contrasts between the synoptic structure of the $\tilde{\chi}$ (200 mb), $\tilde{\psi}_{AV}$ (200 mb), and $\tilde{\psi}_\chi$ (200 mb) fields for various phases of the 30–60 day oscillation of the tropical easterly jet supports the argument that this oscillation is a response of the upper-level monsoon circulation to the eastward-propagating $\tilde{\chi}$ mode.

The last question arose earlier is what the possible impact of this 30–60 day tropical easterly jet is on weather systems of the monsoon region and surrounding areas. The rainfall compiled by Koteswaram (1958) shows that a rain belt lies north of the axis of the tropical easterly jet and east of the Indian subcontinent. In contrast, rainfall is confined to the region south of the jet over Africa. Koteswaram's rainfall distribution over Afrika is in accord with Nicholson's (1981) African rainfall climatology. The contrast of Koteswaram's rainfall distribution on the upstream and downstream sides of the tropical easterly jet is consistent with cross-jet circulation inferred from Chen's (1982) energetics analysis of this jet. The rainfall and weather systems on the upstreamside of the tropical easterly jet are closely related to the Asian monsoon and have been the subjects of extensive studies, as reviewed by Lau and Li (1984). In contrast, the rainfall and weather systems on the downstream side of the tropical easterly jet over the African continent may need more attention.

Tourre (1979) computed the divergence field over the Sahel and contiguous between the low-level African easterly jet and the upper-level tropical easterly jet. He found the mean convergence south of the African easterly jet and the mean convergence north of the tropical easterly jet to be crucial in inducing squall-line activities between these two jets. Constructing squall-line trajectories, Bounoua (1980) found that most of the squall lines over the Sahel are confined by these two jets and

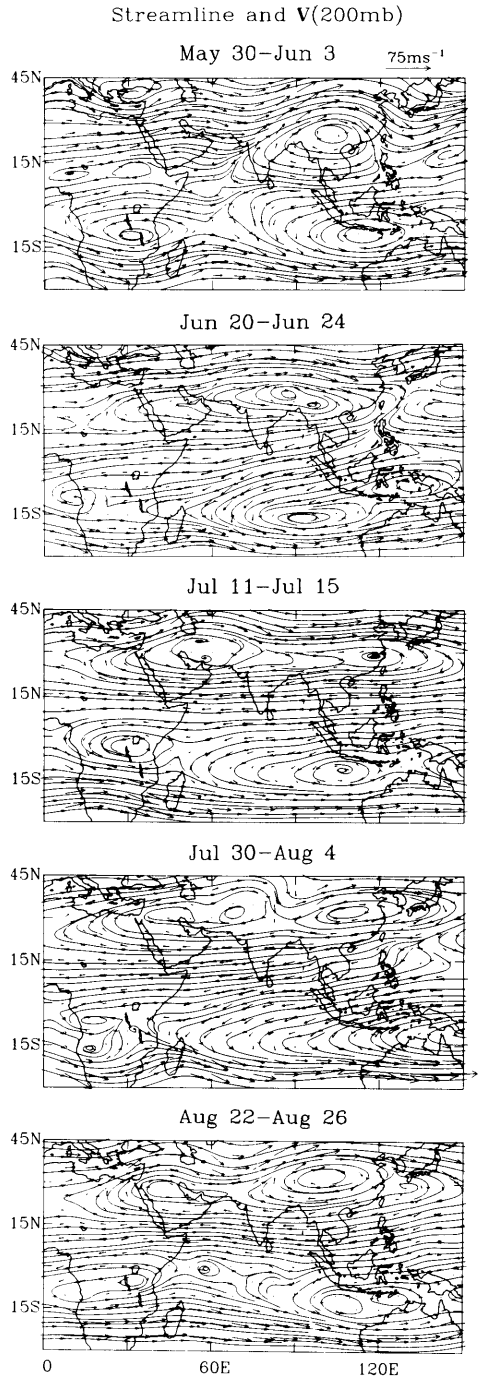

Fig. 8. The 5-day averaged streamlines at 200 mb and V (200 mb) for various phases of the 30–60 day oscillation of the tropical easterly jet.

are responsible for about 70% of the total precipitation over the Sahel. Any fluctuation in location and intensity of these two jets would alter squall-line formation and propagation, and, in turn, the associated Sahelian rainfall. The 5-day mean $\tilde{V}$ (200 mb) synoptic charts shown in Fig. 5 do not seem to exhibit a significant component over equatorial Africa, but the impact of the low-frequency oscillation of the tropical easterly jet on the Sahelian rainfall is far from clear. Further efforts along this line may perhaps be worth pursuing.

The intraseasonal oscillation of the tropical easterly jet may also affect the weather system in some other part of the African continent. The 5-day mean streamlines at 200 mb and V (200 mb) for various phases of the intraseasonal oscillation of the tropical easterly jet (Fig. 8) show some interesting effects of this oscillation on the intensity of the African high. As illustrated in Fig. 8, this high is intensified (weakened) when $\tilde{u}$ (200 mb) (75° E, 0°) reaches its maximum easterly (westerly) anomaly. How the weather systems over central Africa are affected by the oscillation of the African high is beyond the scope of this study and warrants further study.

5. Acknowledgments

This study is supported by NSF Grant ATM-8912451. The major computations of this study were performed on the CRAY-XMP computer of the National Center for Atmospheric Research, which is sponsored by the National Science Foundation. Finally, thanks go to Mrs. Reatha Diedrichs for her typing and to Ms. Anne Richards for her editing.

REFERENCES

Bounoua, L. 1980. *Relation entre champ de vent, genèse et propagation des lignes des grains quest Africâines.* Mémoire de fin d'études, IHFR Oran Algérie.

Cadet, D. L. and Greco, S. 1987. Water vapor transport over the Indian Ocean during 1979 summer. Part I: Water vapor fluxes. *Mon. Wea. Rev. 115*, 653–663.

Chen, T.-C. 1982. On the kinetic energy budget of the summer-mean flow at 200 mb in the tropics. *Tellus 34*, 55–62.

Chen, T.-C. 1985. Global water vapor flux and maintenance during FGGE. *Mon. Wea. Rev. 113*, 1801–1819.

Chen, T.-C. 1989. *Maintenance of the seasonal variation of planetary-scale divergent circulation.* Tech. Rep., Department of Geological and Atmospheric Sciences, Iowa State University, 25 pp (available from author).

Chen, T.-C. and Wiin-Nielsen, A. 1976. On the kinetic energy of the divergent and nondivergent flow in the atmosphere. *Tellus 28*, 486–498.

Chen, T.-C. and Yen, M.-C. 1986. The 40–50 day oscillation of the low-level monsoon circulation over the Indian Ocean. *Mon. Wea. Rev. 114*, 2550–2570.

Chen, T.-C. and van Loon, H. 1987. Interannual variation of the tropical easterly jet. *Mon. Wea. Rev. 115*, 1739–1759.

Chen, T.-C. and Chen, J.-M. 1990. On the maintenance of standing eddies in terms of the stream-function budget analysis. *J. Atmos. Sci. 43*, 2818–2824.

Chen, T.-C., Tzeng, R.-Y. and Yen, M. C. 1988a. Development and life cycle of the Indian monsoon: Effect of the 30–50 day oscillation. *Mon. Wea. Rev. 116*, 2183–2199.

Chen, T.-C., Yen, M.-C. and Murakami, M. 1988b. The water vapor transport associated with the 30–60 day oscillation over the Asian monsoon regions during 1979 summer. *Mon. Wea. Rev. 116*, 1983–2002.

Hartmann, D. L. and Michelsen, M. L. 1989. Intraseasonal periodicities in Indian rainfall. *J. Atmos. Sci. 00*, 2838–2862.

Kang, I. M. and Held, I. M. 1987. Linear and nonlinear diagnostic models of stationary eddies in the upper troposphere during northern summer. *J. Atmos. Sci. 43*, 3045–3057.

Koteswaram, P. 1958. The easterly jet stream in the tropics. *Tellus 10*, 43–57.

Krishnamurti, T. N. and Bahlme, H. N. 1976. Oscillation of a monsoon system. Part I. Observational aspects. *J. Atmos. Sci. 33*, 1937–1954.

Krishnamurti, T. N. and Subrahmanyam, D. 1982. The 30–50 day mode at 850 mb during MONEX. *J. Atmos. Sci. 39*, 2088–2095.

Krishnamurti, T. N. and Ramanathan, Y. 1982. Sensitivity of the monsoon onset to differential heating. *J. Atmos. Sci. 39*, 1290–1306.

Krishnamurti, T. N., Jayakumao, P. K., Sheng, T., Surgi, N. and Kuma, A. 1985. Divergent circulations on the 30 to 50 day time scale. *J. Atmos. Sci. 42*, 364–375.

Lau, K.-M. and Li, M.-T. 1984. The monsoon of East Asia and its global associations. A survey. *Bull. Amer. Meteor. Soc. 65*, 114–125.

Liebmann, B. and Hartmann, D. L. 1981. Interannual variation of outgoing IR association with tropical circulation changes during 1974–1978. *J. Atmos. Sci. 28*, 1153–1162.

Magaña, V. and Yanai, M. 1990. Tropical-midlatitude interaction on the time scale of 30 to 60 days during the northern summer of 1979. *J. Climate*, in press.

Murakami, T., Nakazawa, T. and He, J. 1984a. On the 40–50 day oscillations during the 1979 northern Hemisphere Summer. Part I: Phase propagation. *J. Meteor. Soc. Japan 62*, 440–468.

Murakami, T., Nakazawa, T. and He, J. 1984b. On the 40–50 day oscillation during the 1979 Northern Hemisphere summer. Part II: Heat and moisture budget. *J. Meteor. Soc. Japan 62*, 469–484.

Nicholson, S. E. 1981. Rainfall and atmospheric circulation during drought periods and wetter years in West Africa. *Mon. Wea. Rev. 109*, 2191–2208.

Sikka, D. R. and Gadgil, S. 1980. On the maximum cloud zone and the ITCZ over Indian longitudes during the southeast monsoon. *Mon. Wea. Rev. 108*, 1840–1853.

Tourre, Y. M. 1979. *The squall line over West Africa and tropical eastern Atlantic Ocean during GATE.* Ph.D. dissertation, University of Virginia (available from University Microfilm, Ann Arbor, Michigan).

Young, J. A. 1987. Physics of monsoon: The current view. *Monsoons* (eds. J. S. Fein and P. L. Stephens). John Wiley & Sons, Inc., 211–243.